iScience

CellPress
OPEN ACCESS

Article

Dimethyl fumarate reduces hepatocyte senescence following paracetamol exposure

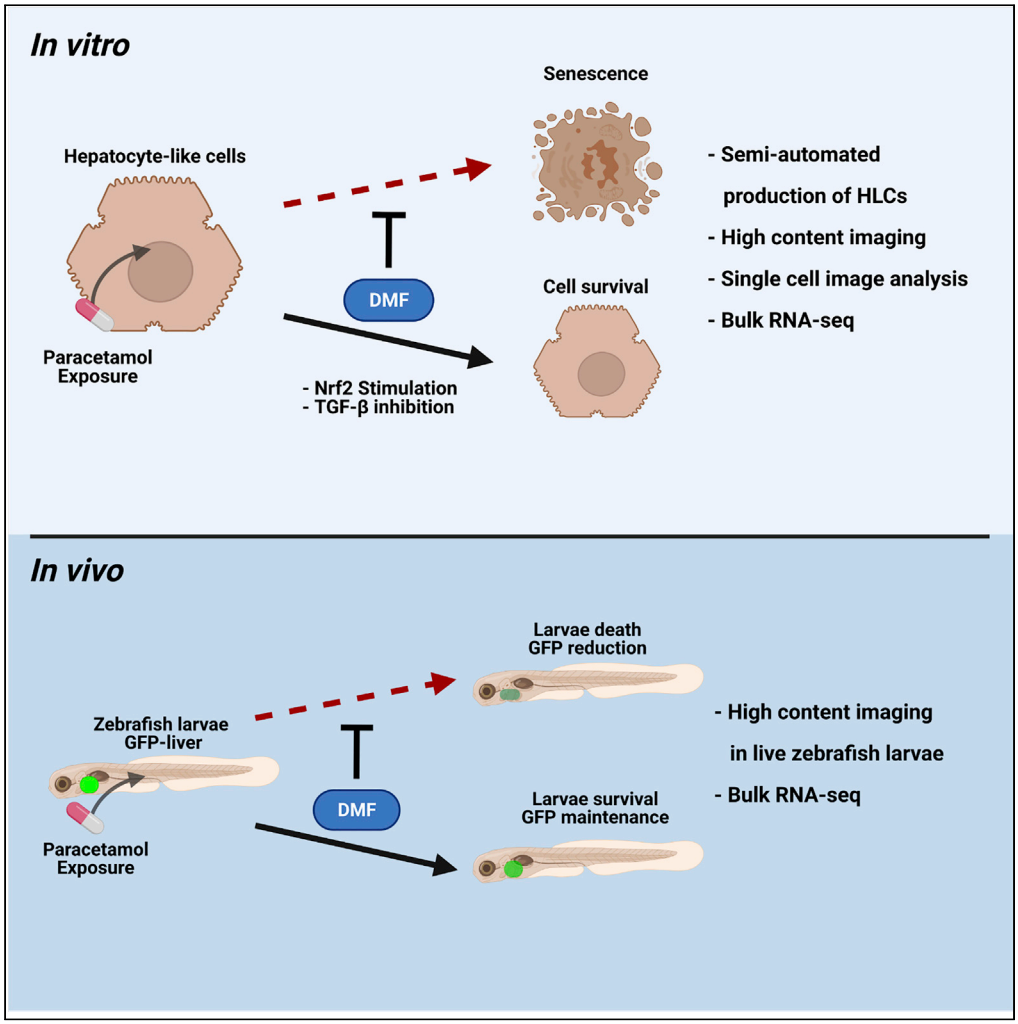

Jose Meseguer-Ripolles, Baltasar Lucendo-Villarin, Carl Tucker, ..., James W. Dear, Jeremy Hughes, David C. Hay

davehay@talktalk.net

Highlights

Dimethyl fumarate protects hepatocyte-like cells from paracetamol-induced stress

Nrf2 activation and TGF-β inhibition are main drivers of cell protection *in vitro*

DMF pre-treatment of zebrafish prevents paracetamol-induced liver injury *in vivo*

Meseguer-Ripolles et al., iScience *24*, 102552
June 25, 2021
https://doi.org/10.1016/j.isci.2021.102552

iScience

CellPress
OPEN ACCESS

Article

Dimethyl fumarate reduces hepatocyte senescence following paracetamol exposure

Jose Meseguer-Ripolles,[1] Baltasar Lucendo-Villarin,[1] Carl Tucker,[2] Sofia Ferreira-Gonzalez,[1] Natalie Homer,[3] Yu Wang,[1] Philip J. Starkey Lewis,[1] Enrique M Toledo,[4,5] Esther Mellado-Gomez,[4,5] Joanna Simpson,[3] Oliver Flint,[1] Himjyot Jaiswal,[4,5] Nicola L. Beer,[4,5] Allan E. Karlsen,[4,5] Stuart J. Forbes,[1] James W. Dear,[3] Jeremy Hughes,[2] and David C. Hay[1,6,*]

SUMMARY

Liver disease is a major cause of premature death. Oxidative stress in the liver represents a key disease driver. Compounds, such as dimethyl fumarate (DMF), can activate the antioxidant response and are used clinically to treat disease. In this study, we tested the protective properties of DMF before or after paracetamol exposure. Following DMF administration, Nrf2 nuclear translocation was tracked at the single-cell level and target gene transactivation confirmed. Next, the protective properties of DMF were examined following paracetamol exposure. Transcriptomic and biochemical analysis revealed that DMF rescue was underpinned by reduced Nf-kB and TGF-β signaling and cell senescence. Following on from these studies, we employed a Zebrafish model to study paracetamol exposure *in vivo*. We combined a genetically modified Zebrafish model, expressing green fluorescent protein exclusively in the liver, with automated microscopy. Pre-treatment with DMF, prior to paracetamol exposure, led to reduced liver damage in Zebrafish demonstrating protective properties.

INTRODUCTION

Drug-induced liver injury (DILI) is a common cause of acute liver failure (ALF) (de Abajo et al., 2004; Tanne, 2006). Paracetamol (acetaminophen)-induced hepatotoxicity is the most common cause of DILI, comprising over 57% of ALF cases in the UK (Bernal and Wendon, 2013). When taken at the recommended level, paracetamol metabolism proceeds mainly via glucuronidation and sulfation (Prescott, 1980, 1983). During an overdose, cytochrome P450 enzymes generate an excess of a highly toxic metabolite, N-acetyl-p-benzoquinone imine (NAPQI) (Dahlin et al., 1984; Gillette et al., 1981; Karthivashan et al., 2015). NAPQI is a highly reactive metabolite that can lead to oxidative stress, hepatocyte death and the induction of senescence (Bird et al., 2018).

Therefore, stimulation of the cell's antioxidant response could reduce the level of hepatocyte injury and promote organ regeneration during DILI. Nuclear factor erythroid-derived 2-like 2 (Nrf2) is a major regulator of the antioxidant and anti-inflammatory response (Hayes and Dinkova-Kostova, 2014). Nrf2 activity is regulated mainly by the Kelch-like ECH-associated protein 1 (Keap1). At rest, Keap1 interacts with Nrf2 forming a complex that undergoes a rapid proteasomal degradation (Itoh et al., 1999). However, upon oxidative stress, the binding capacity of Keap1 is reduced and Nrf2 translocates to the nucleus and transactivates gene expression (Cuadrado et al., 2019). Nrf2's protective effects have been studied in the livers of Nrf2-knockout mice. Those studies highlighted Nrf2's regulatory role in drug metabolism (Aleksunes and Manautou, 2007; Chan et al., 2001; Enomoto et al., 2001) and tissue regeneration (Wakabayashi et al., 2010, p. 1; Zou et al., 2014).

Pharmacological stimulation of the Nrf2 pathway has been proposed as a promising approach to reduce the severity of liver injury in rodents (Xu et al., 2019) and therefore could provide protection for humans. Due to high levels of drug failures, and the timescale of the drug development process, drug repurposing represents an attractive approach to find new therapeutic applications outside their current uses (Pushpakom et al., 2019). With this in mind, we opted to test the protective properties of dimethyl fumarate (DMF), (Gold et al., 2012; Mrowietz et al., 1999), following paracetamol-induced injury, using a stem cell based

[1]Centre for Regenerative Medicine, University of Edinburgh, 5 Little France Drive, Edinburgh EH16 4UU, UK

[2]Centre for Inflammation Research, University of Edinburgh, 47 Little France Drive, Edinburgh EH16 4TJ, UK

[3]Centre for Cardiovascular Science, Queen's Medical Research Institute, University of Edinburgh, 47 Little France Drive, Edinburgh, UK

[4]Novo Nordisk Research Centre Oxford (NNRCO), Novo Nordisk Ltd, Innovation Building - Old Road Campus Roosevelt Drive, OX3 7FZ Oxford, UK

[5]Novo Nordisk Ltd, Novo Nordisk Park 1, 2760 Måløv, Denmark

[6]Lead contact

*Correspondence: davehay@talktalk.net

https://doi.org/10.1016/j.isci.2021.102552

hepatocyte model (Leedale et al., 2021; Meseguer-Ripolles et al., 2018; 2020; Sinton et al., 2021a, 2021b; Wang et al., 2019).

We subsequently compared our *in vitro* findings to a zebrafish model of paracetamol injury. Notably, zebrafish pre-treatment with DMF, prior to paracetamol injury, reduced liver damage and RNA sequencing implied that DMF protection was mediated in part via oxidative stress management. In summary, our work provides new understanding on the protective effects of DMF during paracetamol-induced liver injury *in vitro* and *in vivo* and may serve as useful platform to develop new treatment regimes for patients with drug-induced liver injury.

RESULTS

Activation of the Nrf2 pathway protects hepatocytes from paracetamol-induced stress

PSC-derived hepatocyte-like cells (HLCs) were produced in a 96-well plate in a semi-automated format as previously described (Meseguer-Ripolles et al., 2018). HLCs displayed polygonal-shape and defined cell-to-cell contact. At Day 18, HLCs expressed typical hepatocyte markers and exhibited drug metabolizing Cyp P450 activity (Figure 1). Following incubation of Paracetamol 30 mM for 24 hr, the ability of HLCs to model phase I and II paracetamol metabolism was measured by mass spectrometry. We detected phase II metabolite formation (APAP-Glu and APAP-Sul), as well as Cyp2E1 generated APAP-Cys (2.5 nmol/mL). Notably, APAP-Cys formation was observed at similar levels to patients with paracetamol-induced hepatotoxicity (James et al., 2009) (Table S1).

To understand the effect of HLC exposure to DMF, we exposed cells to 10 μM and 50 μM DMF (Figure S1) (Saidu et al., 2017). In these experiments we also wished to understand if Nrf2 would be activated non-specifically when HLCs were exposed to sudden changes in oxygen or temperature (Gosslau et al., 2001). Non-specific transcription factor activation was marked when HLCs were incubated with H_2O_2 or vehicle, displaying a similar ratio of nuclear/cytoplasmic Nrf2 staining (Figure S2A). To address this, we created a controlled environment by using semi-automated liquid handling systems where non-specific activation of Nrf2 was reduced to a minimum (Figure S2B).

Following incubation with vehicle or DMF, HLCs were stained for Nrf2. The cytoplasm was marked using CellMask and the nucleus using Hoechst. Following this, the levels of Nrf2 nuclear and cytoplasmic localization were extracted at the single-cell level. H_2O_2 was used as a driver of Nrf2 nuclear translocation (Du et al., 2016) and compared to DMF. Following DMF administration, most cells displayed marked Nrf2 nuclear staining with a peak at 2 hr, which was also observed following H_2O_2 treatment. The mean value for the ratio of nuclear/cytoplasmic Nrf2 is 2.23 and 4.05, respectively (Figure 2). DMF-driven Nrf2 translocation was reduced at 6 hr and reached baseline at 24 hr. In contrast, H_2O_2-treated cells displayed Nrf2 nuclear translocation at 24 hr following administration, with a mean value for the ratio of nuclear/cytoplasmic Nrf2 of 1.31 and 4.32 for DMF and H_2O_2, respectively (Figure S1).

Following the establishment of Nrf2 nuclear occupancy, we determined Nrf2-driven gene expression. In line with the positive control, glutathione-disulfide reductase (GSR), NADPH dehydrogenase quinone 1 (NQO1) and heme oxygenase 1 (HMOX1) were significantly induced after DMF treatment (Hayes and Dinkova-Kostova, 2014) (Figure 3A). We then studied the protective properties of DMF in a high concentration model of paracetamol exposure. We opted for this approach as it created a significant level of hepatocellular stress in a 24-hr period Following pre-incubation with DMF (24h), HLCs were then treated with paracetamol 30 mM (24h-48h). Total ATP and Caspase 3/7 induction were quantified. Pre-treatment with both DMF 10 μM and 50 μM significantly reduced ATP loss when compared to paracetamol 30 mM alone. Interestingly, DMF exhibited a concentration-dependent response. HLCs pre-treated with DMF 10 μM displayed a higher level of protection against paracetamol-induced stress when compared with pre-treatment DMF at 50 μM (Figure S3A). Pre-treatment with DMF 10 μM, but not 50 μM, also reduced Caspase 3/7 activity (Figure S3B). Lactate dehydrogenase (LDH) leakage following paracetamol administration was also measured; however no significant changes in LDH levels were detected.

Next, HLCs were exposed to paracetamol for 24h and subsequently treated with DMF (24h-48h). This was to assess the protective effects of DMF following paracetamol exposure. DMF-treated HLCs displayed a significant increase in ATP levels when compared to paracetamol alone (Figure 3C). Next, the ability of DMF to protect hepatocytes from injury was compared to N-acetylcysteine (NAC) (Smilkstein et al., 1988). In addition, a combination of DMF + NAC was performed to determine any potential synergic effects. In

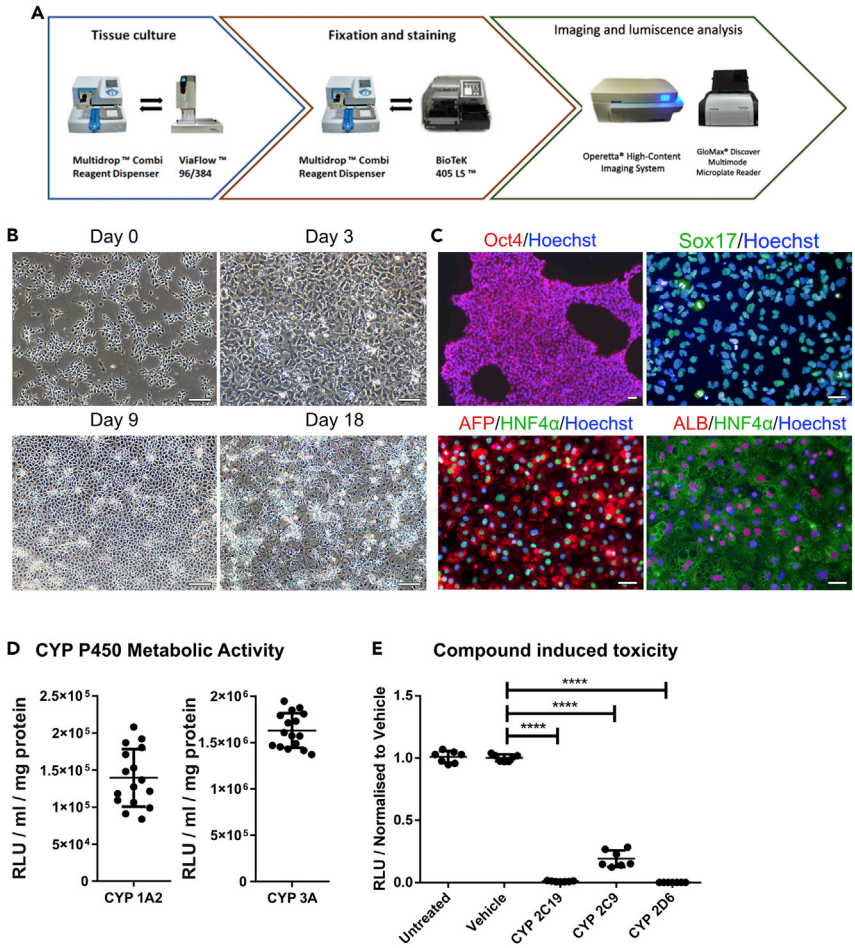

Figure 1. Production and characterization of HLCs

(A) Pipeline overview for automated production of HLCs.

(B) Representative images of cellular morphology during HLC differentiation. hPSCs are seeded as single cells and then driven toward definitive endoderm (Day 3). This is followed by hepatoblast specification characterized by cells displaying cobblestone-like morphology (Day 9). Finally, cells are further differentiated to HLCs acquiring polygonal-shape (Day 18). Scale bar represents 100 μm.

(C) Immunostaining of the different stages of the differentiation. hPSC cells express the pluripotent marker Oct4 (Day 0). Definitive endoderm marker Sox17 expression was detected at Day 3. Hepatic progenitor specification was evidenced by HNF4α and AFP protein expression (Day 9). Finally, HLC differentiation was evidenced by HNF4α and ALB expression (Day 18). Scale bar represents 50 μm.

(D) Basal cytochrome P450 activity of HLCs was determined at Day 18. CYP 3A and CYP 1A2 activity were measured by luminescence, and activity is quoted as relative light units (RLUs)/mL per mg of protein. Dot plot represents n = 16. Data are represented as mean ± SEM.

(E) Day 18 HLCs were exposed to BMS compounds (48 hr) with specificity for particular cytochrome P450 enzymes. Following incubation, ATP levels were quantified. ATP levels are represented as relative light units (RLUs) normalized to the vehicle. Dot plot represents n = 6. One-way ANOVA test and post-hoc Tukey multiple-comparison test was used. ****$p < 0.0001$. Data are represented as mean ± SEM.

the pre-treatment group, DMF, NAC or a combination of both were administered for 24 hr, prior to exposure of paracetamol (from 24h-48h) (Figure 3B). This was compared to a model, where DMF, NAC, or the combination were administered 24 hours after paracetamol treatment (Figure 3C). Assessment of the protective effects was analyzed by total ATP production. In all cases, DMF treatment resulted in significant increases in ATP content when compared to paracetamol alone. NAC treatment also showed a significant increase in ATP when compared to paracetamol treated cells in the pre-treatment group only. Using a combination of DMF and NAC led to significant increases in ATP levels in both tretatment groups.

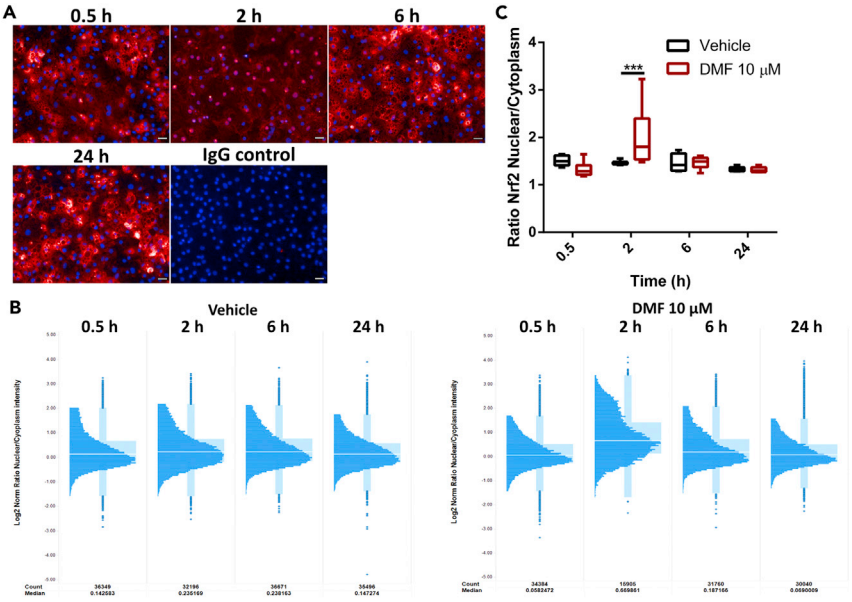

Figure 2. Nrf2 nuclear translocation dynamics upon stimulation

(A) Nrf2 nuclear translocation following DMF administration. Day 18 HLCs were treated with 10 μM DMF for 0.5,2, 6, and 24 hr. After treatment cells were immunostained for Nrf2. Representative images from each time point are provided. Scale bar represents 50 μm.

(B) Single-cell analysis of Nrf2 dynamics upon DMF or vehicle administration. Ratio of Nrf2 nuclear translocation following DMF administration. Box plot, where each timepoint is represented in a box plot with a histogram to show the sample distribution. The white line represents the median of the sample.

(C) Nuclear localization of the Nrf2 per time point and condition. n = 4. One-way ANOVA test and post-hoc Tukey multiple-comparison test was used ***$p < 0.001$. Box plot were whiskers represent Min to Max.

Validation of these experiments was performed via morphological profiling using a modified version of the Cell Painting assay (Bray et al., 2016). Following paracetamol exposure, in both pre- and post-treatment models, HLCs were stained with NucBlue for the nuclei, Cell Mask green for the cytoplasm and Mitotracker for the mitochondria, and subsequently imaged using the operetta high content microscope. Using cell segmentation, 86 different image-based features were used to create a morphological profile (Figure S4). Python script was written for min-max data normalization and sample clustering. Unbiased clustering of the different treatments were conducted using morphological profiling (Figure S4). Principal component analysis (PCA) was performed for data reduction. In the pre-treatment experiment, the paracetamol exposed group displayed a distinct cell profile phenotype to the other groups (Figure 3D). In the post-treatment experiment, paracetamol-treated HLCs displayed a marked cell profile when compared to vehicle. When HLCs where treated with DMF after paracetamol injury, HLC cell profile phenotype shifted closer to the vehicle group implying improved cell health (Figure 3D) (Figure S4).

Transcriptomic analysis of paracetamol-induced stress and protection

To provide more detail on cell toxicity and DMF protection, transcriptomic analyses were performed for both the pre- and post-treatment groups. Gene Set Enrichment Analysis (GSEA) was used in combination with the molecular signatures database (MSigDB) for the analysis of key biological processes (Liberzon et al., 2015). In the pre-treatment group, GSEA-MSigDB analysis showed the enrichment in multiple pathways including adipogenesis, xenobiotic metabolism, oxidative phosphorylation or fatty acid metabolism. It also showed a reduction in TNF-α signaling via Nf-kB, epithelial mesenchymal transition, apical junction, or apoptosis (Figure 4, Table S2). The post-treatment group GSEA-MSigDB analysis showed the enrichment in multiple pathways, including interferon alpha response, bile acid, fatty acid, and xenobiotic metabolism. In addition, there was a reduction in several hallmark pathways associated with cellular senescence and apoptosis including TNF-α signaling via Nf-kB, MYC targets, TGF-β signaling pathway, P53 pathway, and inflammatory response (Figure 5, Table S3).

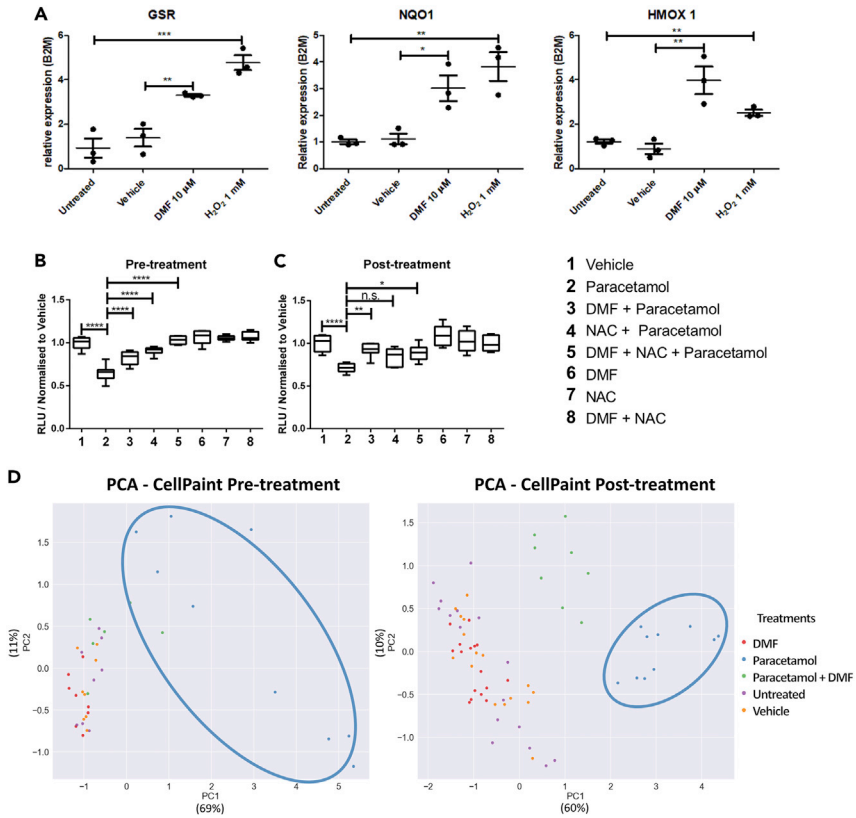

Figure 3. DMF stimulates Nrf2 and protects HLCs from paracetamol-induced injury

(A) Nrf2 target gene expression following DMF (10 μM) or H_2O_2 (1mM) treatment for 3h. The three target genes tested, HMOX1, NQO1, and GSR were upregulated following treatment with either DMF or H_2O_2. HMOX1 = heme oxygenase 1, NQO1 = NAD(P)H quinone dehydrogenase 1, GSR = glutathione-disulfide reductase. n = 3. Data ploteed as a dot plot with mean ± SEM. One-way ANOVA test and post-hoc Tukey multiple-comparison test was used. *p < 0.05, **p < 0.01, ***p < 0.001.

(B) Pre-treatment of HLCs with DMF (10 μM), NAC (1 mM) or combination of the two for 24 hr prior to the administration of paracetamol (30mM) for 24 hr, shows increased levels of ATP compared to paracetamol treatment alone. n = 6. One-way ANOVA test and post-hoc Tukey multiple-comparison test was used. ****p < 0.0001. Box plot were whiskers represent Min to Max.

(C) Post-treatment of DMF (10 μM) after a 24-hr incubation with paracetamol (30mM) shows increased levels of ATP when compared to paracetamol treatment alone. n = 6. One-way ANOVA test and post-hoc Tukey multiple-comparison test was used.*p < 0.05, **p < 0.01, ****p < 0.0001. Box plot were whiskers represent Min to Max.

(D) DMF pre-treatment assessment by Cell Paint profiling. The PCA plot takes account of the different features and compares the different populations.

DMF prevents paracetamol-induced senescence in HLCs

TFG-β-induced senescence has been shown as one the main drivers of hepatic failure after paracetamol overdose. In the post-treatment group, gene expression analysis highlighted the inhibition of TGF-β signaling upon DMF treatment was detected as one of the main protective events (Figure 5, Table S3). To validate this finding, HLCs were treated with the TFG-β receptor inhibitor SB-431542 following paracetamol injury (Watabe et al., 2003). Both DMF and SB-431542 treatment increased cell viability when compared to paracetamol alone (Figure 6A). To address the effects of this treatment on the levels of cellular senescence, we measured p16 expression in HLCs after paracetamol injury. Following 24 h incubation of paracetamol, HLCs were exposed to either DMF or SB-431542 for 6 h. Following fixation and staining, p16 nuclear expression was examined at single-cell level (Figure 6B). HLCs treated with paracetamol alone displayed a significant increase in p16 nuclear localization when compared to the vehicle control, whereas both DMF- and SB-431542-treated HLCs exhibited reduced expression and nuclear occupancy of p16 (Figure 6C). Additionally, DMF and SB-431542 after treatment resulted in reduced cell loss when compared to HLCs treated with paracetamol alone (Figure 6D). These results suggest that

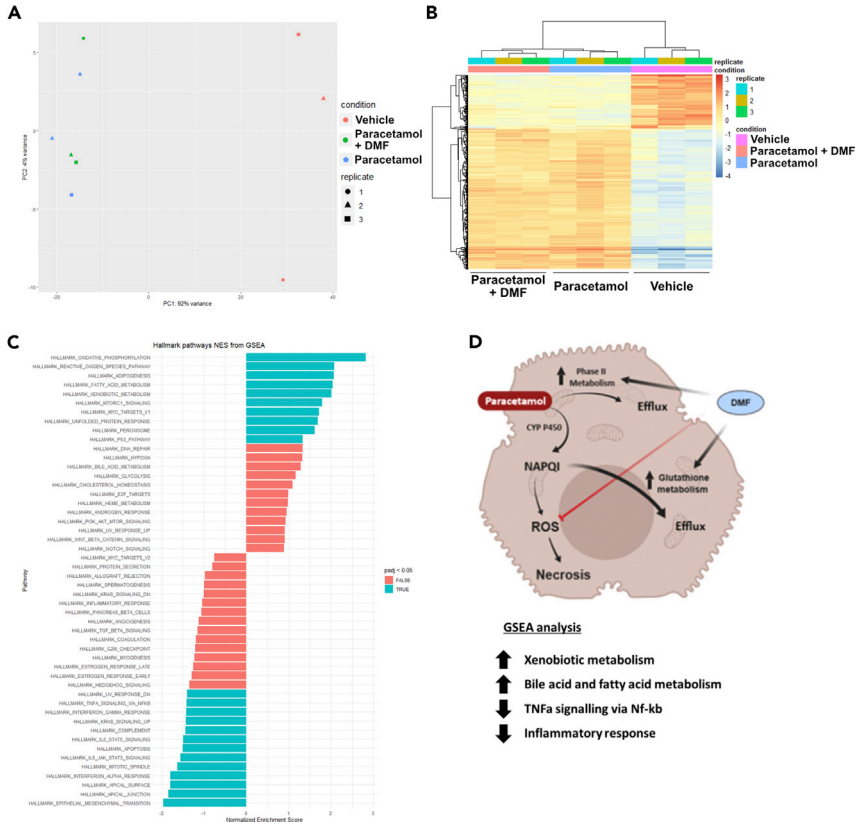

Figure 4. Transcriptomic analysis reveals protective effect of DMF pre-treatment in HLCs

(A) PCA plot of HLC treatment and clustering. The colors are used for the different groups, and the shape for each replicate.

(B) Replicate variability assessment using heatmap visualization in the pre-treatment group.

(C) GSEA-MSigDB enrichment analysis from HLCs pre-treatment RNA-seq data set. The graph displays the normalized enrichment score from the 50 hallmarks, and these hallmarks are representative of important biological processes. Labeled in blue are labeled are the hallmarks with an adjusted p value <0.05.

(D) Proposed mechanism of action of DMF protection following pre-treatment. N = 3 (8 replicates per experiment, 24 replicates in total).

DMF protection could prevent induction of cell senescence induction via the inhibition of TGF-β signaling.

Assessment of DMF treatment in a Zebrafish model of paracetamol injury

Zebrafish larvae were used to study the protective effect of DMF treatment in an *in vivo* model of paracetamol injury. Two different Zebrafish lines were used for these studies. The wild-type line, WIK, was used for assay optimization (Figure 7A). Wild-type Zebrafish embryos at 3 Days postfertilization (d.p.f.) were pre-treated with DMF (2.5 μM) or vehicle (dimethyl sulfoxide) for 6 h prior to paracetamol treatment (10 mM) for a further 42 h. After treatment, survival was determined by both mobility and heartbeat of the larvae. An embryo was marked as dead if no mobility or heartbeat were detected. Notably, DMF pre-treatment significantly improved larvae survival when compared to paracetamol-only treated larvae (Figure 7A).

Assay refinement and automation using genetically modified zebrafish and microscopy

Following these experiments, we employed a genetically modified zebrafish line which expresses GFP in the liver (Tg(-2.8fabp10a:GFP). The GFP reporter in the Tg(-2.8fabp10a:GFP) line is under the control of the liver-type fatty acid-binding protein (FABP10A) promoter, which is only expressed in hepatocytes. By combining the optical properties of the zebrafish with a liver specific reporter line, liver damage after paracetamol exposure could be measured by the reduction of GFP fluorescence (Vliegenthart et al., 2017). This

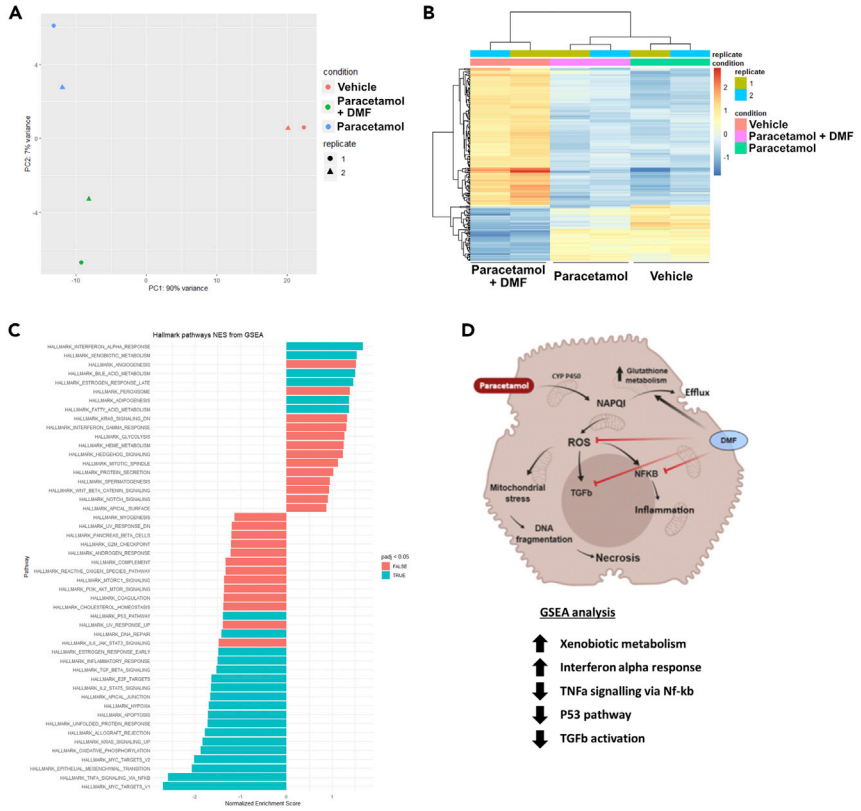

Figure 5. Transcriptomic analysis reveals protective mechanism of DMF post-treatment in HLCs

(A) PCA plot of HLC treatment and clustering. The colors are used for the different groups, and the shape for each replicate.

(B) Replicate variability assessment using heatmap visualization in the post-treatment group.

(C) GSEA-MSigDB enrichment analysis from HLCs post-treatment RNA-seq data set. The graph displays the normalized enrichment score from the 50 hallmarks, and these hallmarks are representative of important biological processes. Labeled in blue are labeled are the hallmarks with an adjusted p value <0.05.

(D) Proposed mechanism of action of DMF protection following post-treatment. N = 2 (8 replicates combined per experiment, 16 replicates in total).

line was used to scale-up the assay and quantify changes in GFP fluorescence following liver injury (Her et al., 2003; Vliegenthart et al., 2017). The zebrafish experiments were performed at 3 d.p.f following zebrafish hatching. Experiments were terminated 5 d.p.f. in accordance with Home Office Regulations. Two different methods were developed for measuring fluorescence intensity. The first system was a live imaging high-throughput platform using the Operetta microscope, whereas the second uses a plate reader to measure total larva fluorescence emission.

For the live imaging, after paracetamol exposure, single larvae were embedded in agarose 0.75% wt/vol in a 96-well plate. Following embedding, imaging was performed to assess system performance. Due to the high variability in terms of orientation and plane focusing, an orientation tool developed by Wittbrodt et al. was 3D printed and used in our studies (Figure S5) (Wittbrodt et al., 2014). To fabricate the agarose plates, 0.75%, wt/vol agar was added into the 96-well plate following the positioning of the orientation tool. Once the agar solidified, the orientation tool was removed creating a 'V' shape in the agar, facilitating reproducible larvae positioning in terms of focus plane and orientation (Figure 7B).

Following zebrafish positioning standardization, a supervised machine learning algorithm was developed for automatic zebrafish larva detection following automatic GFP+ liver segmentation and fluorescence quantification (Figure 7C). First, manual annotation of both fish and background was uploaded into the algorithm (Figure 7C). Following fish identification, selection of the larvae region of interest (ROI) was performed based on shape and intensity features (Figure 7C). After fish segmentation, liver detection was

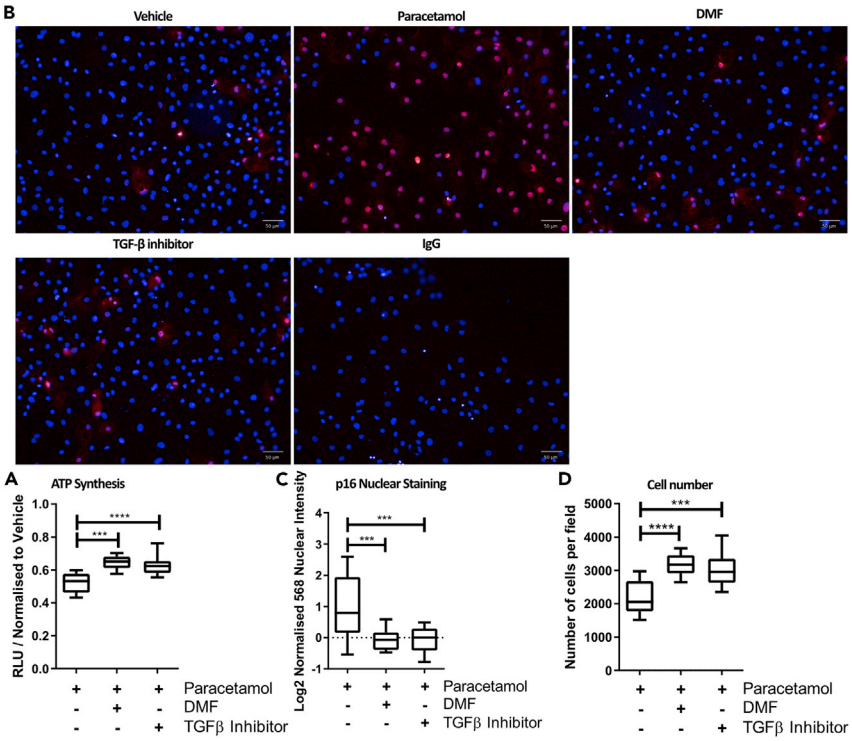

Figure 6. DMF treatment following paracetamol exposure reduces p16 expression in HLCs

(A) 24 hr treatment of DMF (10 μM) or SB-431542 (10 μM), following 24 hparacetamol (30 mM) exposure, improved ATP levels in HLCs. n = 12. One-way ANOVA test and post-hoc Tukey multiple-comparison test was used. **p < 0.01, ***p < 0.001. Box plot were whiskers represent Min to Max.

(B) 6 hr treatment of DMF (10 μM) or SB-431542 (10μM) following 24 hr paracetamol (30 mM) exposure reduces p16 expression and nuclear staining in HLCs. Scale bar represents 50 μm.

(C) Single-cell image analysis quantification of p16 shows a significant increase of p16 nuclear intensity when HLCs are treated with paracetamol (30 mM) alone. n = >6. One-way ANOVA test and post-hoc Tukey multiple-comparison test was used. ***p < 0.001. Box plot were whiskers represent Min to Max.

(D) Treatment with DMF (10 μM) or SB-431542 (10 μM) for 6 hr following 24hr paracetamol (30 mM) exposure for 24 hr significantly prevented cell loss. n = >6. One-way ANOVA test and post-hoc Tukey multiple-comparison test was used. ***p < 0.001 ****p < 0.0001. Scale bar represents 50μm. Box plot were whiskers represent Min to Max.

performed using a similar approach (Figure 7C). This system allows a fast and unbiased quantification of liver GFP intensity. In parallel with automated image analysis, we developed a plate reader assay to detect GFP fluorescence. To test both assays performance, the GFP reporting zebrafish single embryos per well were placed into a black 96-well plate and exposed to paracetamol. Following this, fluorescence quantification was performed using both methods of analysis. In both systems, paracetamol-induced liver damage resulted in a significant loss of GFP fluorescence (Figures 7D and 7E). In contrast, larvae that were pre-treated with DMF (2.5 μM) displayed increased levels of GFP fluorescence (Figures 7D and 7E).

Zebrafish transcriptomic analysis following paracetamol exposure +/- DMF pre-treatment

In order to study transcriptomic changes that took place following paracetamol exposure, we employed RNA sequencing. PCA analysis with two components was used to visualize gene expression differences between paracetamol- and paracetamol plus DMF-treated larvae (Figure S6). A heatmap of the top 200 most variable genes was prepared for sample hierarchical clustering (Figure S7). Following data refinement, differential expression analysis was performed using DESeq2. The detection threshold applied was adjusted (p value >0.05 and log2 Fold Change ±0.58). During the analysis, 9395 genes displayed low counts and it was not possible to include them in the analysis. Fifty-three percent of the total counts passed the quality control required for DEseq2 analysis. Comparing the DMF pre-treated paracetamol treated group to the paracetamol-only group, 30 genes were upregulated and 10 were downregulated (Table S4). From the upregulated DEGs, the top 5 include: transcobalamin beta a (tcnba), several members of the crystallin family (crygm), and conting, CABZ01080568

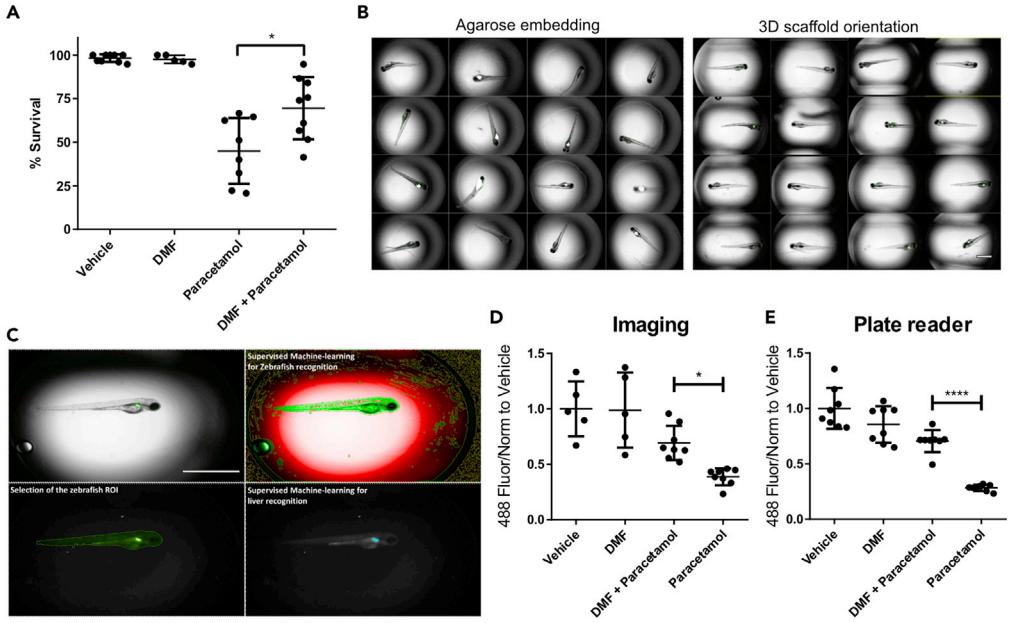

Figure 7. DMF protects zebrafish from paracetamol-induced injury

(A) WIK-larvae were treated with vehicle, and DMF (2.5uM) for 48 hr. The other experimental groups were treated with either vehicle or DMF (2.5uM) for 6 hr, prior to treatment with paracetamol (10mM) for a further 42 hr. Each dot represents the survival percentage of a biological replicate (30–35 zebrafish). Data ploteed as a dot plot with mean ± SEM. n=>5. One-way ANOVA test and post-hoc Tukey multiple-comparison test was used. *$p < 0.05$.

(B) Methods for larvae orientation for live imaging. Plates that employ manual agarose embedding, demonstrate random distributions of larvae with focal variation. Plates prepared using the 3D scaffold orientation tool generates a reproducible system in terms of larvae position, focal plane, and spatial orientation. Scale bar represents 1 mm.

(C) Supervised machine learning was used for automatic zebrafish recognition. Pixel texture was used to exclude background (red) from zebrafish (green) following refinement by size and shape. Selection of ROI based on shape and size of the larvae was used to distinguish between larvae and background. Next, supervised machine learning was used for GFP-positive liver recognition. Scale bar represents 1 mm.

(D) Loss of GFP signal following 42 hr of paracetamol exposure was quantified using high content imaging. Wild-type lines were used to detect any potential issues with autofluorescence. n=>6. One-way ANOVA test and post-hoc Tukey multiple-comparison test was used. *$p < 0.05$. Data ploteed as a dot plot with mean ± SEM.

(E) Loss of GFP signal following 42 hr of paracetamol exposure was measured using a plate reader. n=>3. One-way ANOVA test and post-hoc Tukey multiple-comparison test was used. ****$p < 0.0001$. Data ploteed as a dot plot with mean ± SEM.

(Table S4). Downregulated DEGs included 3-hydroxyanthranilate 3, 4- dioxygenase (haao), the LOC100149563 which is homologous to the human gene HtrA serine peptidase 2 (HTRA2), F-Box Protein 32 (fbxo32) and apolipoprotein Da, duplicate 1 (apoda.1), and retinoid isomerohydrolase (rpe65a) (Table S4). Finally, zebrafish genes were converted into human homologs and GSEA-MSigDB analysis was performed. There was a positive enrichment in multiple pathways including MYC targets, oxidative phosphorylation, reactive oxygen species pathway, DNA repair, apoptosis and G2M checkpoint. There were no significant hallmark decreases (Figure 8).

DISCUSSION

Paracetamol-induced hepatotoxicity is one of the most common causes of DILI in the Western world (Tanne, 2006). It is characterized by extensive hepatocyte death in the liver due to an excess of toxic metabolite formation (Williams et al., 2014). Recent reports indicate that following the initial injury, the remaining hepatocytes can enter a senescent state, driven by TGB-β1 activation (Bird et al., 2018). This prevents the hepatocytes from restoring organ mass and functioning, leading to liver failure in the patient. NAC is the current treatment option for paracetamol overdose, with optimal effects in patients when used within the first 8-10 h (Harrison et al., 1990; Keays et al., 1991; Smilkstein et al., 1988). Many patients present outside this window, when NAC has less marked effects. Therefore, new approaches that work for longer periods of time are required.

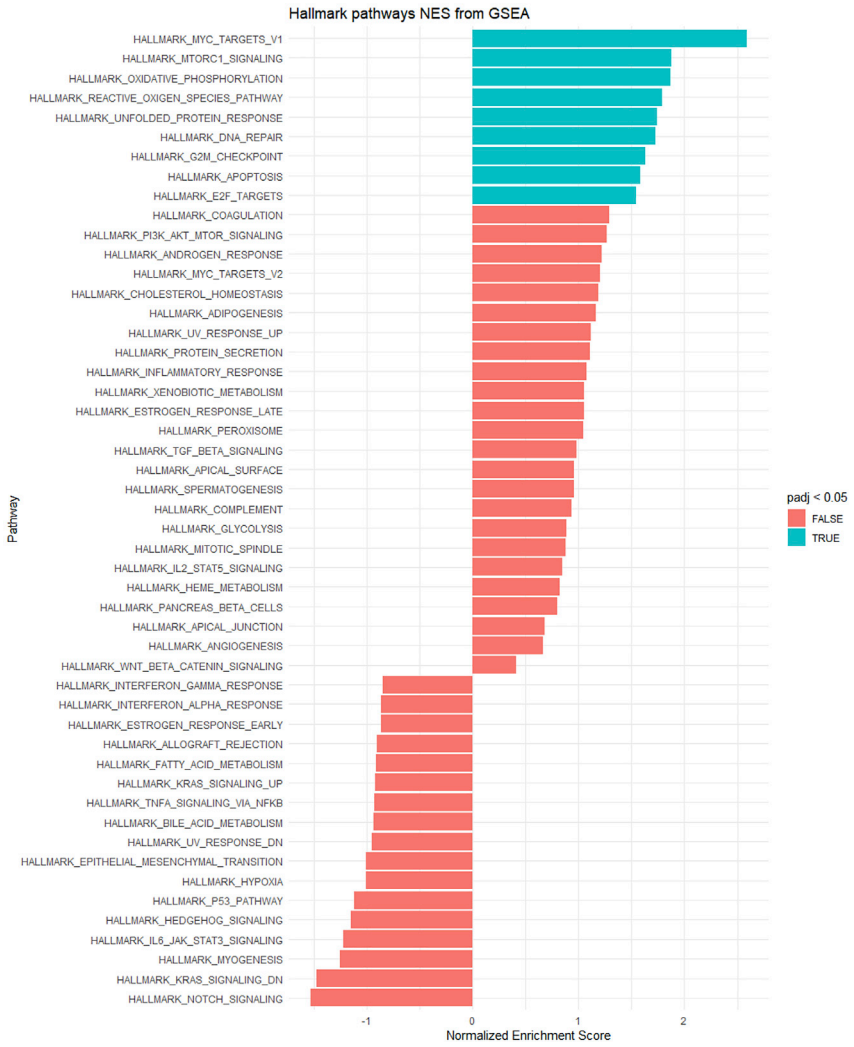

Figure 8. GSEA-MSigDB enrichment analysis from the zebrafish RNA-seq data set

Graph represents the normalized enrichment score from the 50 hallmarks, and these hallmarks are representative of important biological processes. This score is obtained by combining all the gene expression information when comparing zebrafish larvae treated with paracetamol + DMF vs paracetamol. In blue are labeled the hallmarks with an adjusted p value <0.05.

The activation of the Nrf2 pathway is vital to the liver's ability to deal with oxidative stress. In support of this recent work reported that pharmacological activation of Nrf2 with TBE-31 reversed non-alcoholic steatohepatitis in mice (Sharma et al., 2018). These changes were not observed in Nrf2-null mice, representing a promising strategy to reduce liver damage. It is also known that DMF stimulates anti-inflammatory and immunomodulatory effects, effected in part by Nrf2 transcriptional activation (Ruggieri et al., 2014; Wu et al., 2017). The protective effects of DMF were recently reported in a paracetamol injury model (Abdelrahman and Abdel-Rahman, 2019). Although DMF demonstrated protection following paracetamol exposure, the timepoints tested had limited relevance to the clinic.

In our studies, the protective properties of DMF were studied in two different scenarios, pre- and post-paracetamol exposure. We acknowledge that DMF pre-treatment is clinically irrelevant, but it was important to understand that active Nrf2 in our system was capable of transactivating gene expression. We opted to use a concentration of 10 μM in our studies as it fell within the dose range used to treat multiple sclerosis (Ruggieri et al., 2014). At higher concentrations, DMF treatment did not yield protective effects, likely due to an increase of oxidative stress (Saidu et al., 2017). In the context of drug overdose, DMF administration 24 hr

post-paracetamol exposure resulted in increased ATP levels. To elucidate the potential protective effect(s) of DMF, mRNA sequencing (RNA-seq) and proof of concept experimentation were performed.

Interestingly, in the post-treatment group, downregulation of pro-injury pathways (NF-kB and TGF-β) was observed. Our findings are consistent with previous studies in cancer cells demonstrating that DMF blocks NF-kB activation by covalently modifying p65 and blocking the DNA binding activity (Kastrati et al., 2016; Loewe et al., 2002). In addition, DMF-mediated Nrf2 activation has been shown to block TGF-β1 activation by interacting and blocking Smad3 protein activity in a model of renal fibrosis (Oh et al., 2012a). Therefore, we hypothesized that DMF protection in the post-treatment scenario is likely due to suppression of inflammatory gene expression. This was further validated using a TGF-β receptor inhibitor (SB-431542), which provided protection from paracetamol-induced stress in our system.

Injury-induced senescence in hepatocytes follows paracetamol intoxication. This represents a key factor of liver failure. Senescent hepatocytes are able to spread their phenotype to the surrounding healthy tissue, thus actively blocking regeneration and function (Bird et al., 2018). Following paracetamol-induced injury in HLCs, we examined the expression of a key factor in the onset and maintenance of the senescent phenotype, p16 (Malavolta et al., 2018; Rayess et al., 2012). In the presence of DMF and SB-431542 (6hr) following paracetamol exposure, we observed reduced expression and nuclear translocation of p16. These results suggest that the protective properties of DMF in HLCs could be mediated in part by inhibiting TGF-β-driven senescence.

It should be noted, that pharmacological activation of Nrf2 in the liver during paracetamol exposure would not only affect hepatocytes in the liver. In support of this, the use of the Nrf2 inducer, sulforaphane, results in reduced human stellate cell (HSC) activation and transdifferentiation (Oh et al., 2012b). Whereas, Nrf2 silencing in primary HSCs led to their activation (Prestigiacomo and Suter-Dick, 2018). There are also immune related complications during acute liver injury (Woolbright and Jaeschke, 2017). Of note, the activation of Nrf2 suppresses the macrophage inflammatory response by blocking the transcription of pro inflammatory cytokines via an ARE activation independent mechanism (Kobayashi et al., 2016). Therefore, DMF administration could enhance liver regeneration by protecting multiple cell types in the liver.

With this in mind, we studied the protective effects of DMF pre-treatment in a genetically modified zebrafish model. We employed zebrafish models as they express Nrf2 paralog genes and allow for rapid assessment of liver damage. Following the establishment of paracetamol-induced toxicity and DMF's protective effect in the WIK-larvae, we opted to use the Tg(-2.8fabp10a:GFP) transgenic zebrafish line and high content imaging for further experiments (Vliegenthart et al., 2017). The use of the Tg(-2.8fabp10a:GFP) line allows the user to study liver volume following paracetamol exposure (North et al., 2010; Vliegenthart et al., 2017). As a control, we employed total fluorescence quantification in single embryos using a plate reader. We demonstrate that paracetamol treatment reduced zebrafish survival and GFP fluorescence. However, the pre-treatment of Zebrafish with DMF (6 hr), prior to paracetamol administration, prevented loss in GFP fluorescence and improved larvae survival.

From these results, we propose that the protective effects from DMF pre-treatment in zebrafish are due from the modulation of multiple pathways. First, DMF-treated zebrafish showed an increase in metabolism and cell proliferation, and this could be due to an Nrf2 activation. Even though we did not observe Nrf2 target gene upregulation, likely as a result of the experimental design, the induction of LXR pathway involved in the crystallin expression may represent Nrf2 activation (Yan et al., 2018). DMF pre-treatment also led to reduced development of cell apoptosis (HTRA2), which could have been mediated in part by p53 and TGF-β signaling (Haupt et al., 2003; Song, 2007).

In summary, we have built *in vitro* and *in vivo* technologies to investigate the protective role of DMF in the context of paracetamol-induced liver injury. We report the protective effects of DMF *in vitro* and *in vivo*, implicating key cell signaling pathways and processes, such as senescence. These findings may have clinical relevance and provide a solid platform to build future *in vivo* studies upon.

Limitations of the study

Although the semi-automated differentiation platform allows rapid and reproducible production of HLCs, further improvements are required to better recapitulate the *in vivo* situation. This could be achieved by using iPSC-derived HLCs that recapitulate wider genetic diversity and the use of 3D spheroids containing

multiple cell types from the liver (Lucendo-Villarin et al., 2020; Meseguer-Ripolles et al., 2021). The Nrf2 studies could also be improved by using gene editing to produce a Nrf2 reporter line which would facilitate the real-time study of Nrf2 protein biology and gene transactivation. Further study of the interaction between DMF and cellular senescence, in the context of paracetamol-induced hepatotoxicity, should be undertaken *in vitro* and *in vivo* to capture multi-cellular and multi-organ effects. Care should be taken when interpreting the zebrafish GSEA analysis as the data set was designed to analyze human data (Liberzon et al., 2015). Additionally, the multi-organ effects of paracetamol and DMF treatment were not analysed in this work with all studies performed in whole Zebrafish larvae.

STAR★METHODS

Detailed methods are provided in the online version of this paper and include the following:

- KEY RESOURCES TABLE
- RESOURCE AVAILABILITY
  - Lead contact
  - Materials availability
  - Data and code availability
- EXPERIMENTAL MODEL AND DETAILS
  - Human ESC culture
  - Zebrafish experiments
- METHOD DETAILS
  - Bioinformatic analysis
  - Cell culture and differentiation
  - Cell Paint assay and morphological profiling
  - Cell viability and caspase 3/7 assay
  - CYP P450 activity
  - Differential expression analysis
  - High content imaging and analysis
  - Immunofluorescence
  - Mass spectrometry
  - mRNA extraction and sequencing
  - Orientation tool for zebrafish imaging 3D printing
  - Reagent preparation for HLC incubation
  - RNA extraction and qPCR
  - DMF + paracetamol treatment time points
  - Zebrafish lines and husbandry
  - Zebrafish chemical exposure
  - Zebrafish high-throughput live imaging
  - Zebrafish plate reader fluorescence quantification
  - Zebrafish RNA isolation and characterization
- QUANTIFICATION AND STATISTICAL ANALYSIS
  - Statistical analysis

SUPPLEMENTAL INFORMATION

Supplemental information can be found online at https://doi.org/10.1016/j.isci.2021.102552.

ACKNOWLEDGMENTS

This study was supported with awards from the MRC Doctoral Training Partnership (MR/K501293/1) and the Chief Scientist Office (TCS/16/37). We are grateful to Dr Eoghan O'Duibhir for his assistance with the cell phenotyping work.

AUTHOR CONTRIBUTIONS

J.M.-R was involved in conceptualization, experimental design, validation, data analysis, data curation, writing (original draft preparation, reviewing, and editing) and visualization. B.L.V., S.F.G., Y.W., and P.J.S.-L. were involved in methodology, validation, formal analysis, and experimental design. E.M.T., E.M.G., and H.J. were involved in RNA-seq library preparation, sequencing, and pre-analysis. C.T. was involved in zebrafish

maintenance. N.H. was involved in mass spectrometry sample processing and analysis. N.B., A.E.K., S.J.F., J.W.D., J.H., and D.C.H. were involved in conceptualization, methodology, experimental design, formal analysis, provision of resources, writing (reviewing and editing), project administration, funding acquisition, and supervision.

DECLARATION OF INTERESTS

D.C.H is a co-founder and shareholder of Stemnovate Ltd. J.M.-R. and P.J.S.-L. are presently employed at Resolution Therapeutics. E.M.T., E.M.G., H.J., N.B. and A.E.K. are/were employees of Novo Nordisk Ltd. The rest of the authors certify that they have no conflicts of interest in the subject matter or materials discussed in this article. D.C.H. is serving as a guest editor on a special issue for iScience in 2021, and this issue is not related to the current article.

Received: February 17, 2021
Revised: April 7, 2021
Accepted: May 14, 2021
Published: June 25, 2021

REFERENCES

Abdelrahman, R.S., and Abdel-Rahman, N. (2019). Dimethyl fumarate ameliorates acetaminophen-induced hepatic injury in mice dependent of Nrf-2/HO-1 pathway. Life Sci. *217*, 251–260. https://doi.org/10.1016/j.lfs.2018.12.013.

Aleksunes, L.M., and Manautou, J.E. (2007). Emerging role of Nrf2 in protecting against hepatic and gastrointestinal disease. Toxicol. Pathol. *35*, 459–473. https://doi.org/10.1080/01926230701311344.

Bernal, W., and Wendon, J. (2013). Acute liver failure. New Engl. J. Med. *369*, 2525–2534. https://doi.org/10.1056/NEJMra1208937.

Bird, T.G., Müller, M., Boulter, L., Vincent, D.F., Ridgway, R.A., Lopez-Guadamillas, E., Lu, W.-Y., Jamieson, T., Govaere, O., Campbell, A.D., et al. (2018). TGFβ inhibition restores a regenerative response in acute liver injury by suppressing paracrine senescence. Sci. Transl. Med. *10*. https://doi.org/10.1126/scitranslmed.aan1230.

Bray, M.-A., Singh, S., Han, H., Davis, C.T., Borgeson, B., Hartland, C., Kost-Alimova, M., Gustafsdottir, S.M., Gibson, C.C., and Carpenter, A.E. (2016). Cell Painting, a high-content image-based assay for morphological profiling using multiplexed fluorescent dyes. Nat. Protoc. *11*, 1757–1774. https://doi.org/10.1038/nprot.2016.105.

Chan, K., Han, X.D., and Kan, Y.W. (2001). An important function of Nrf2 in combating oxidative stress: detoxification of acetaminophen. Proc. Natl. Acad. Sci. U S A *98*, 4611–4616. https://doi.org/10.1073/pnas.081082098.

Cuadrado, A., Rojo, A.I., Wells, G., Hayes, J.D., Cousin, S.P., Rumsey, W.L., Attucks, O.C., Franklin, S., Levonen, A.-L., Kensler, T.W., and Dinkova-Kostova, A.T. (2019). Therapeutic targeting of the NRF2 and KEAP1 partnership in chronic diseases. Nat. Rev. Drug Discov. *18*, 295. https://doi.org/10.1038/s41573-018-0008-x.

Dahlin, D.C., Miwa, G.T., Lu, A.Y., and Nelson, S.D. (1984). N-acetyl-p-benzoquinone imine: a cytochrome P-450-mediated oxidation product of acetaminophen. Proc. Natl. Acad. Sci. U S A *81*, 1327–1331.

de Abajo, F.J., Montero, D., Madurga, M., and Rodríguez, L.A.G. (2004). Acute and clinically relevant drug-induced liver injury: a population based case-control study. Br. J. Clin. Pharmacol. *58*, 71–80. https://doi.org/10.1111/j.1365-2125.2004.02133.x.

Du, K., Ramachandran, A., and Jaeschke, H. (2016). Oxidative stress during acetaminophen hepatotoxicity: sources, pathophysiological role and therapeutic potential. Redox Biol. *10*, 148–156. https://doi.org/10.1016/j.redox.2016.10.001.

Enomoto, A., Itoh, K., Nagayoshi, E., Haruta, J., Kimura, T., O'Connor, T., Harada, T., and Yamamoto, M. (2001). High sensitivity of Nrf2 knockout mice to acetaminophen hepatotoxicity associated with decreased expression of ARE-regulated drug metabolizing enzymes and antioxidant genes. Toxicol. Sci. *59*, 169–177. https://doi.org/10.1093/toxsci/59.1.169.

Gillette, J.R., Nelson, S.D., Mulder, G.J., Jollow, D.J., Mitchell, J.R., Pohl, L.R., and Hinson, J.A. (1981). Formation of chemically reactive metabolites of phenacetin and acetaminophen. Adv. Exp. Med. Biol. *136*, 931–950.

Gold, R., Kappos, L., Arnold, D.L., Bar-Or, A., Giovannoni, G., Selmaj, K., Tornatore, C., Sweetser, M.T., Yang, M., Sheikh, S.I., and Dawson, K.T. (2012). Placebo-controlled phase 3 study of oral BG-12 for relapsing multiple sclerosis. New Engl. J. Med. *367*, 1098–1107. https://doi.org/10.1056/NEJMoa1114287.

Gosslau, A., Ruoff, P., Mohsenzadeh, S., Hobohm, U., and Rensing, L. (2001). Heat shock and oxidative stress-induced exposure of hydrophobic protein domains as common signal in the induction ofhsp68. J. Biol. Chem. *276*, 1814–1821. https://doi.org/10.1074/jbc.M008280200.

Harrison, P.M., Keays, R., Bray, G.P., Alexander, G.J., and Williams, R. (1990). Improved outcome of paracetamol-induced fulminant hepatic failure by late administration of acetylcysteine. Lancet *335*, 1572–1573. https://doi.org/10.1016/0140-6736(90)91388-q.

Haupt, S., Berger, M., Goldberg, Z., and Haupt, Y. (2003). Apoptosis—the p53 network. J. Cell Sci. *116*, 4077–4085. https://doi.org/10.1242/jcs.00739.

Hayes, J.D., and Dinkova-Kostova, A.T. (2014). The Nrf2 regulatory network provides an interface between redox and intermediary metabolism. Trends Biochem. Sci. *39*, 199–218. https://doi.org/10.1016/j.tibs.2014.02.002.

Her, G.M., Chiang, C.-C., Chen, W.-Y., and Wu, J.-L. (2003). In vivo studies of liver-type fatty acid binding protein (L-FABP) gene expression in liver of transgenic zebrafish (Danio rerio). FEBS Lett. *538*, 125–133.

Itoh, K., Wakabayashi, N., Katoh, Y., Ishii, T., Igarashi, K., Engel, J.D., and Yamamoto, M. (1999). Keap1 represses nuclear activation of antioxidant responsive elements by Nrf2 through binding to the amino-terminal Neh2 domain. Genes Dev *13*, 76–86.

James, L.P., Letzig, L., Simpson, P.M., Capparelli, E., Roberts, D.W., Hinson, J.A., Davern, T.J., and Lee, W.M. (2009). Pharmacokinetics of acetaminophen-protein adducts in adults with acetaminophen overdose and acute liver failure. Drug Metab. Dispos. *37*, 1779–1784. https://doi.org/10.1124/dmd.108.026195.

Karthivashan, G., Arulselvan, P., and Fakurazi, S. (2015). Pathways involved in acetaminophen hepatotoxicity with specific targets for inhibition/downregulation. RSC Adv. *5*, 62040–62051. https://doi.org/10.1039/C5RA07838E.

Kastrati, I., Siklos, M.I., Calderon-Gierszal, E.L., El-Shennawy, L., Georgieva, G., Thayer, E.N., Thatcher, G.R.J., and Frasor, J. (2016). Dimethyl fumarate inhibits the nuclear factor κB pathway in breast cancer cells by covalent modification of p65 protein. J. Biol. Chem. *291*, 3639–3647. https://doi.org/10.1074/jbc.M115.679704.

Keays, R., Harrison, P.M., Wendon, J.A., Forbes, A., Gove, C., Alexander, G.J., and Williams, R. (1991). Intravenous acetylcysteine in paracetamol

induced fulminant hepatic failure: a prospective controlled trial. BMJ *303*, 1026–1029. https://doi.org/10.1136/bmj.303.6809.1026.

Kobayashi, E.H., Suzuki, T., Funayama, R., Nagashima, T., Hayashi, M., Sekine, H., Tanaka, N., Moriguchi, T., Motohashi, H., Nakayama, K., and Yamamoto, M. (2016). Nrf2 suppresses macrophage inflammatory response by blocking proinflammatory cytokine transcription. Nat. Commun. *7*, 11624. https://doi.org/10.1038/ncomms11624.

Leedale, J.A., Lucendo-Villarin, B., Meseguer-Ripolles, J., Kasarinaite, A., Webb, S.D., and Hay, D.C. (2021). Mathematical modelling of oxygen gradients in stem cell-derived liver tissue. PLoS One *16*, e0244070. https://doi.org/10.1371/journal.pone.0244070.

Liberzon, A., Birger, C., Thorvaldsdóttir, H., Ghandi, M., Mesirov, J.P., and Tamayo, P. (2015). The molecular signatures database hallmark gene set collection. Cell Syst. *1*, 417–425. https://doi.org/10.1016/j.cels.2015.12.004.

Loewe, R., Holnthoner, W., Gröger, M., Pillinger, M., Gruber, F., Mechtcheriakova, D., Hofer, E., Wolff, K., and Petzelbauer, P. (2002). Dimethylfumarate inhibits TNF-induced nuclear entry of NF-κB/p65 in human endothelial cells. J. Immunol. *168*, 4781–4787. https://doi.org/10.4049/jimmunol.168.9.4781.

Love, M.I., Huber, W., and Anders, S. (2014). Moderated estimation of fold change and dispersion for RNA-seq data with DESeq2. Genome Biol. *15*, 550. https://doi.org/10.1186/s13059-014-0550-8.

Lucendo-Villarin, B., Meseguer-Ripolles, J., Drew, J., Fischer, L., Ma, E., Flint, O., Simpson, K.J., Machesky, L.M., Mountford, J.C., and Hay, D.C. (2020). Development of a cost-effective automated platform to produce human liver spheroids for basic and applied research. Biofabrication *13*, 015009. https://doi.org/10.1088/1758-5090/abbdb2.

Malavolta, M., Bracci, M., Santarelli, L., Sayeed, M.A., Pierpaoli, E., Giacconi, R., Costarelli, L., Piacenza, F., Basso, A., Cardelli, M., and Provinciali, M. (2018). Inducers of senescence, toxic compounds, and senolytics: the multiple faces of nrf2-activating phytochemicals in cancer adjuvant therapy. Mediators Inflamm. *2018*. https://doi.org/10.1155/2018/4159013.

Meseguer-Ripolles, J., Kasarinaite, A., Lucendo-Villarin, B., and Hay, D.C. (2021). Protocol for automated production of human stem cell derived liver spheres. STAR Protoc. *2*, 100502. https://doi.org/10.1016/j.xpro.2021.100502.

Meseguer-Ripolles, J., Lucendo-Villarin, B., Wang, Y., and Hay, D.C. (2018). Semi-automated production of hepatocyte like cells from pluripotent stem cells. J. Vis. Exp. *137*, e57995. https://doi.org/10.3791/57995.

Meseguer-Ripolles, J., Wang, Y., Sorteberg, A., Sharma, A., Ding, N.-L., Lucendo-Villarin, B., Kramer, P., Segeritz, C.-P., and Hay, D.C. (2020). Hepatic progenitor specification from pluripotent stem cells using a defined differentiation system. J. Vis. Exp. *159*, e61256. https://doi.org/10.3791/61256.

Mrowietz, U., Christophers, E., and Altmeyer, P. (1999). Treatment of severe psoriasis with fumaric acid esters: scientific background and guidelines for therapeutic use. The German Fumaric Acid Ester Consensus Conference. Br. J. Dermatol. *141*, 424–429.

North, T.E., Babu, I.R., Vedder, L.M., Lord, A.M., Wishnok, J.S., Tannenbaum, S.R., Zon, L.I., and Goessling, W. (2010). PGE2-regulated wnt signaling and N-acetylcysteine are synergistically hepatoprotective in zebrafish acetaminophen injury. Proc. Natl. Acad. Sci. U S A *107*, 17315–17320. https://doi.org/10.1073/pnas.1008209107.

Oh, C.J., Kim, J.-Y., Choi, Y.-K., Kim, H.-J., Jeong, J.-Y., Bae, K.-H., Park, K.-G., and Lee, I.-K. (2012a). Dimethylfumarate attenuates renal fibrosis via NF-E2-related factor 2-mediated inhibition of transforming growth factor-β/Smad signaling. PLoS One *7*, e45870. https://doi.org/10.1371/journal.pone.0045870.

Oh, C.J., Kim, J.-Y., Min, A.-K., Park, K.-G., Harris, R.A., Kim, H.-J., and Lee, I.-K. (2012b). Sulforaphane attenuates hepatic fibrosis via NF-E2-related factor 2-mediated inhibition of transforming growth factor-β/Smad signaling. Free Radic. Biol. Med. *52*, 671–682. https://doi.org/10.1016/j.freeradbiomed.2011.11.012.

Prescott. (1980). Kinetics and metabolism of paracetamol and phenacetin. Br J Clin Pharmacol. *10* (*Suppl 2*). https://doi.org/10.1111/j.1365-2125.1980.tb01812.x.

Prescott. (1983). Paracetamol overdosage. Pharmacological considerations and clinical management. Drugs Mar *25*, 290–314. https://doi.org/10.2165/00003495-198325030-00002.

Prestigiacomo, V., and Suter-Dick, L. (2018). Nrf2 protects stellate cells from Smad-dependent cell activation. PLoS One *13*. https://doi.org/10.1371/journal.pone.0201044.

Pushpakom, S., Iorio, F., Eyers, P.A., Escott, K.J., Hopper, S., Wells, A., Doig, A., Guilliams, T., Latimer, J., McNamee, C., et al. (2019). Drug repurposing: progress, challenges and recommendations. Nat. Rev. Drug Discov. *18*, 41–58. https://doi.org/10.1038/nrd.2018.168.

Quackenbush, J. (2002). Microarray data normalization and transformation. Nat. Genet. *32*, 496–501. https://doi.org/10.1038/ng1032.

Rayess, H., Wang, M.B., and Srivatsan, E.S. (2012). Cellular senescence and tumor suppressor gene p16. Int. J. Cancer *130*, 1715–1725. https://doi.org/10.1002/ijc.27316.

Ruggieri, S., Tortorella, C., and Gasperini, C. (2014). Pharmacology and clinical efficacy of dimethyl fumarate (BG-12) for treatment of relapsing–remitting multiple sclerosis. Ther. Clin. Risk Manage. *10*, 229–239. https://doi.org/10.2147/TCRM.S53285.

Saidu, N.E.B., Noé, G., Cerles, O., Cabel, L., Kavian-Tessler, N., Chouzenoux, S., Bahuaud, M., Chéreau, C., Nicco, C., Leroy, K., et al. (2017). Dimethyl fumarate controls the NRF2/DJ-1 Axis in cancer cells: therapeutic applications. Mol. Cancer Ther. *16*, 529–539. https://doi.org/10.1158/1535-7163.MCT-16-0405.

Sharma, R.S., Harrison, D.J., Kisielewski, D., Cassidy, D.M., McNeilly, A.D., Gallagher, J.R., Walsh, S.V., Honda, T., McCrimmon, R.J., Dinkova-Kostova, A.T., et al. (2018). Experimental nonalcoholic steatohepatitis and liver fibrosis are ameliorated by pharmacologic activation of Nrf2 (NF-E2 p45-related factor 2). Cell Mol. Gastroenterol. Hepatol. *5*, 367–398. https://doi.org/10.1016/j.jcmgh.2017.11.016.

Sinton, M.C., Meseguer-Ripolles, J., Lucendo-Villarin, B., Drake, A.J., and Hay, D.C. (2021a). Modeling human hepatic steatosis in pluripotent stem cell-derived hepatocytes. STAR Protoc. *2*, 100493. https://doi.org/10.1016/j.xpro.2021.100493.

Sinton, M.C., Meseguer-Ripolles, J., Lucendo-Villarin, B., Wernig-Zorc, S., Thomson, J.P., Carter, R.N., Lyall, M.J., Walker, P.D., Thakker, A., Meehan, R.R., et al. (2021b). A human pluripotent stem cell model for the analysis of metabolic dysfunction in hepatic steatosis. iScience *24*, 101931. https://doi.org/10.1016/j.isci.2020.101931.

Smilkstein, M.J., Knapp, G.L., Kulig, K.W., and Rumack, B.H. (1988). Efficacy of oral N-acetylcysteine in the treatment of acetaminophen overdose. Analysis of the national multicenter study (1976 to 1985). New Engl. J. Med. *319*, 1557–1562. https://doi.org/10.1056/NEJM198812153192401.

Song, J. (2007). EMT or apoptosis: a decision for TGF-β. Cell Res. *17*, 289–290. https://doi.org/10.1038/cr.2007.25.

Subramanian, A., Tamayo, P., Mootha, V.K., Mukherjee, S., Ebert, B.L., Gillette, M.A., Paulovich, A., Pomeroy, S.L., Golub, T.R., Lander, E.S., and Mesirov, J.P. (2005). Gene set enrichment analysis: a knowledge-based approach for interpreting genome-wide expression profiles. Proc. Natl. Acad. Sci. U S A *102*, 15545–15550. https://doi.org/10.1073/pnas.0506580102.

Tanne, J. (2006). Paracetamol causes most liver failure in UK and US. BMJ *332*, 628.

Vliegenthart, A.D.B., Wei, C., Buckley, C., Berends, C., de Potter, C.M.J., Schneemann, S., Del Pozo, J., Tucker, C., Mullins, J.J., Webb, D.J., and Dear, J.W. (2017). Characterization of triptolide-induced hepatotoxicity by imaging and transcriptomics in a novel zebrafish model. Toxicol. Sci. *159*, 380–391. https://doi.org/10.1093/toxsci/kfx144.

Wakabayashi, N., Shin, S., Slocum, S.L., Agoston, E.S., Wakabayashi, J., Kwak, M.-K., Misra, V., Biswal, S., Yamamoto, M., and Kensler, T.W. (2010). Regulation of Notch1 signaling by Nrf2: implications for tissue regeneration. Sci. Signal. *3*, ra52. https://doi.org/10.1126/scisignal.2000762.

Wang, Y., Alhaque, S., Cameron, K., Meseguer-Ripolles, J., Lucendo-Villarin, B., Rashidi, H., and Hay, D.C. (2017). Defined and scalable generation of hepatocyte-like cells from human pluripotent stem cells. J. Vis. Exp. *121*, e55355. https://doi.org/10.3791/55355.

Wang, Y., Tatham, M.H., Schmidt-Heck, W., Swann, C., Singh-Dolt, K., Meseguer-Ripolles, J., Lucendo-Villarin, B., Kunath, T., Rudd, T.R., Smith,

A.J.H., et al. (2019). Multiomics analyses of HNF4α protein domain function during human pluripotent stem cell differentiation. iScience *16*, 206–217. https://doi.org/10.1016/j.isci.2019.05.028.

Watabe, T., Nishihara, A., Mishima, K., Yamashita, J., Shimizu, K., Miyazawa, K., Nishikawa, S.-I., and Miyazono, K. (2003). TGF-beta receptor kinase inhibitor enhances growth and integrity of embryonic stem cell-derived endothelial cells. J. Cell Biol. *163*, 1303–1311. https://doi.org/10.1083/jcb.200305147.

Williams, R., Aspinall, R., Bellis, M., Camps-Walsh, G., Cramp, M., Dhawan, A., Ferguson, J., Forton, D., Foster, G., Gilmore, I., et al. (2014). Addressing liver disease in the UK: a blueprint for attaining excellence in health care and reducing premature mortality from lifestyle issues of excess consumption of alcohol, obesity, and viral hepatitis. Lancet *384*, 1953–1997. https://doi.org/10.1016/S0140-6736(14)61838-9.

Wittbrodt, J.N., Liebel, U., and Gehrig, J. (2014). Generation of orientation tools for automated zebrafish screening assays using desktop 3D printing. BMC Biotechnol. *14*, 36. https://doi.org/10.1186/1472-6750-14-36.

Woolbright, B.L., and Jaeschke, H. (2017). Role of the inflammasome in acetaminophen-induced liver injury and acute liver failure. J. Hepatol. *66*, 836–848. https://doi.org/10.1016/j.jhep.2016.11.017.

Wu, Q., Wang, Q., Mao, G., Dowling, C.A., Lundy, S.K., and Mao-Draayer, Y. (2017). Dimethyl fumarate selectively reduces memory T cells and shifts the balance between Th1/Th17 and Th2 in multiple sclerosis patients. J. Immunol. *198*, 3069–3080. https://doi.org/10.4049/jimmunol.1601532.

Xu, D., Xu, M., Jeong, S., Qian, Y., Wu, H., Xia, Q., and Kong, X. (2019). The role of Nrf2 in liver disease: novel molecular mechanisms and therapeutic approaches. Front. Pharmacol. *9*. https://doi.org/10.3389/fphar.2018.01428.

Yan, C., Zhang, Y., Zhang, X., Aa, J., Wang, G., and Xie, Y. (2018). Curcumin regulates endogenous and exogenous metabolism via Nrf2-FXR-LXR pathway in NAFLD mice. Biomed. Pharmacother. *105*, 274–281. https://doi.org/10.1016/j.biopha.2018.05.135.

Zou, Y., Lee, J., Nambiar, S.M., Hu, M., Rui, W., Bao, Q., Chan, J.Y., and Dai, G. (2014). Nrf2 is involved in maintaining hepatocyte identity during liver regeneration. PLoS One *9*, e107423. https://doi.org/10.1371/journal.pone.0107423.

STAR★METHODS

KEY RESOURCES TABLE

REAGENT or RESOURCE	SOURCE	IDENTIFIER
Antibodies		
Albumin 1:200 (mouse)	Sigma-Aldrich	Cat#A6684 - RRID:AB_258309
Alpha-fetoprotein 1:500 (mouse)	Abcam	Cat#ab3980 - RRID:AB_304203
Anti-goat 488 (secondary antibody) 1:400	Life technologies	Cat#A-11055 - RRID:AB_2534102
Anti-Mouse 488 (secondary antibody) 1:400	Life technologies	Cat#A-11001 - RRID:AB_2534069
Anti-Mouse 568 (secondary antibody) 1:400	Life technologies	Cat#A-11004 - RRID:AB_2534072
Anti-rabbit 488 (secondary antibody) 1:400	Life technologies	Cat#A-11008 - RRID:AB_143165
Anti-rabbit 568 (secondary antibody) 1:400	Life technologies	Cat#A-11011 - RRID:AB_143157
HNF-4α 1:400 (rabbit)	Santa Cruz	Cat#sc-8987 - RRID:AB_2116913
IgG 1:400	Vector	Cat# I-2000-1, I-5000-5, I-1000-5 / RRID:AB_2336354, RRID:AB_2336353, RRID:AB_2336355
Nrf2 1:100 (rabbit)	Abcam	Cat#ab31163 - RRID:AB_881705
Oct4 1:200 (Rabbit)	Abcam	Cat#ab19857 - RRID:AB_445175
p16 1:1000 (Rabbit)	Abcam	Cat#Ab108349 - RRID:AB_10858268
Sox17 1:200 (Goat)	R&D Systems, Inc.	Cat#AF1924 - RRID:AB_355060
Chemicals, peptides, and recombinant proteins		
B27	Life Technologies	Cat#12587-010
Bovine Serum Albumin	Sigma-Aldrich	Cat#A2058
Dimethyl Fumarate	Sigma	Cat#624-49-7
Dimethyl sulfoxide, DMSO	Life Technologies	Cat#D5879
GlutaMAX-I	Life Technologies	Cat#35050-038
HCS CellMask™	Invitrogen	Cat#H32714
Hepatocyte growth factor	Peprotech	Cat#100-39
Human recombinant laminin 521	Biolamina	Cat#LN521-02
Hydrocortisone- 21 hemisuccinate sodium salt	Sigma-Aldrich	Cat#H4881-1G
Hydrogen peroxide solution	Sigma	Cat#7722-84-1
Minimal essential medium Non-Essentail Amino Acids	Life Technologies	Cat#11140-035
MitoTracker™ Deep Red FM - Special Packaging	Invitrogen	Cat#M22426
NucBlue Live ReadyProbes® Reagent	Molecular Probes	Cat#R37605
Paracetamol	Sigma	Cat#103-90-2
Paraformaldehyde (4% wt/vol)	Electron Microscopy Sciences	Cat#15710-S
Penicillin-Streptomycin (10,000 U/ml)	Life Technologies	Cat#15140-122
Recombinant Human/Mouse/Rat Activin A Protein	R&D	Cat#338-AC
Rho-associated Kinase (ROCK) Inhibitor Y27632	Tocris Bioscience	Cat#1254
SB 431542	Tocris	Cat#1614
TWEEN 20	Sigma	Cat# P9416
Wnt3a	R&D	Cat#1324-WN/CF
B-mercaptoethanol	Life Technologies	Cat#31350-010

(*Continued on next page*)

Continued

REAGENT or RESOURCE	SOURCE	IDENTIFIER
Critical commercial assays		
BCA Protein Assay Kit	ThermoFisher	Cat#23225
Caspase-Glo® 3/7 Assay System	Promega	Cat# G8091
CellTiter-Glo® Luminescent Cell Viability Assay	Promega	Cat# G7571
Dynabeads mRNA DIRECT Purification Kit	ThermoFisher	Cat#61012
High Sensitivity RNA ScreenTape	Agilent	Cat#5067- 5579
High Sensitivity RNA ScreenTape Buffer	Agilent	Cat#5067- 5580
miRNeasy mini Kit	Qiagen	Cat#217004
P450-Glo CYP1A2 Assay and Screening System	Promega	Cat#V8771
P450-Glo CYP3A4 Assay and Screening System	Promega	Cat# V8801
QuantiTect Reverse Transcription Kit	Qiagen	Cat#205311
QuantSeq 3′ mRNA-Seq Library Prep Kit FWD for Illumina	Lexogen	Cat#015
Qubit™ RNA HS Assay Kit	ThermoFisher	Cat# Q32852
RNeasy mini Kit	Qiagen	Cat#74104
Experimental models: Cell lines		
Human Embryonic Stem Cell Line H9	WiCell	Ca#WA09
Software and algorithms		
Columbus software	PerkinElmer	https://www.perkinelmer.com/uk/product/image-data-storage-and-analysis-system-columbus
Tibco Spotfire	Tibco Spotfire	https://www.tibco.com/products/tibco-spotfire
Other		
2200 TapeStation system	Aligent	Cat#G2964AA
DPBS with Calcium and Magnesium	ThermoFisher	Cat#14040133
DPBS, no calcium, no magnesium	ThermoFisher	Cat#14190250
Gentle cell dissociation reagent	STEMCELL Technologies	Cat#7174
GloMax explorer multiplex plate reader	Promega	Cat#GM3500
GripTips for VIAFLO 96	Integra	Cat#6434
HepatoZYME-SFM	Life Techonolgies	Cat#17705-021
Human Endothelial-SFM	ThermoFisher	Cat#11111044
Knockout DMEM	Life Technologies	Cat# 10829-018
KO-SR (Knockout serum replacement)	Life Technologies	Cat#10828-028
mTeSR1 medium	STEMCELL Technologies	Cat#85850
MultidropCombi Reagent Dispenser	ThermoFisher	Cat#5840300
Operetta High-Content Imaging System	PerkinElmer	Cat#HH12000000
RPMI 1640	Life Technologies	Cat#11875-093
Small Cell Scraper, Non-pyrogenic, Sterile	Corning Incorporated Costar	Cat#3010
Standard tube dispensing cassette	ThermoFisher	Cat#24072670
VIAFLO 96 Electronic 96-channel pipette	Integra	Cat#6001
White plates for CYP assays	Greiner Bio-One	Cat#655075

RESOURCE AVAILABILITY

Lead contact

David C Hay: Centre for Regenerative Medicine, University of Edinburgh, 5 Little France Drive, Edinburgh, EH16 4UU. davehay@talktalk.net.

Materials availability

This study did not generate new unique reagents.

Data and code availability

The data and code reported in this paper has been deposited to Mendeley Data: https://dx.doi.org/10.17632/6my37k5bb8.1

EXPERIMENTAL MODEL AND DETAILS

Human ESC culture

This study was performed using the female embryonic stem cell line H9 (see key resource table for details). H9 human pluripotent stem cell was purchased from WiCell Research Institute. H9 PSC were cultured and differentiated using standard procedures (Wang et al., 2017). hPSC maintenance was performed on pre-coated laminin-521 (Biolamina) in mTeSR1 (STEMCELL technologies) at 37°C, 5% CO_2.

Zebrafish experiments

We employed a genetically modified Zebrafish model, which expresses green fluorescent protein (GFP) exclusively in the liver (Vliegenthart et al., 2017). Upon liver damage the GFP signal was lost allowing the quantitatively determination of liver damage *in vivo* following paracetamol exposure.

METHOD DETAILS

Bioinformatic analysis

Single-cell imaging analysis for the Nrf2 nuclear translocation quantification was performed using Spotfire software for data annotation, visualization and analysis. Data analysis from the Cell Paint assay was performed using Python script. RNA-seq analysis was performed in R using with the DEseq2 packages (Love et al., 2014).

Cell culture and differentiation

H9 and P106 human pluripotent stem cells were cultured and differentiated using standard procedures (Wang et al., 2017). hPSC maintenance was performed on pre-coated laminin-521 (Biolamina) in mTeSR1 (STEMCELL technologies) at 37°C, 5% CO_2. For HLCs differentiation, hPSC were seeded in a single-cell suspension at 50000 cells/cm^2. Differentiation was started when cells reached 40% confluence by replacing the medium with definitive endoderm differentiation medium: RPMI 1640 containing 1× B27 (Life Technologies), 100 ng/mL Activin A (PeproTech), and 50 ng/mL Wnt3a (R&D Systems). The medium was changed every 24 h for 72 h. On day 3, endoderm differentiation medium was replaced by the hepatoblast differentiation medium which was renewed every second day for 5 days. The medium consisted of knockout (KO)-DMEM (Life Technologies), Serum replacement (Life Technologies), 0.5% Glutamax (Life Technologies), 1% non-essential amino acids (Life Technologies), 0.2% β-mercaptoethanol (Life Technologies), and 1% DMSO (Sigma). At day 8, hepatoblast were cultured for additional 10 days in the hepatocyte maturation medium consisting of HepatoZYME (Life Technologies) containing 1% Glutamax (Life Technologies), supplemented with 10 ng/mL hepatocyte growth factor (PeproTech) and 20 ng/mL oncostatin M (PeproTech). HLCs were produced in a 96-well plate format using a semi-automated pipeline using an automated platform (Meseguer-Ripolles et al., 2018).

Cell Paint assay and morphological profiling

Following HLCs treatment, cells were fixed using 4% paraformaldehyde for 15 min. Next, cells were stained for cytoplasm (CellMask 488nm, ThermoFisher), mitochondria (Mitotracker 665nm, ThermoFisher) and nuclei (NucBlue 460 nm, ThermoFisher) according to manufacturers' instructions. Morphological profiling was performed by image cell segmentation. First cell nuclei were defined using Hoechst. Next, cytoplasm was identified using CellMask staining from the nuclei identified previously. After cells have been identify automatically, a quality control step was performed to remove incorrect object segmentations. Then, by

measuring the cell number, intensities, morphologies and pixel texture from the different channels a morphological profile was created using 86 different features. This was used to define changes in cells upon different stimuli (Bray et al., 2016).

Cell viability and caspase 3/7 assay

Cell viability was determined by the amount of ATP in HLCs differentiated in 96-well plate format measured using CellTiter-Glo® Luminescent Cell Viability assay (Promega). Caspase 3/7 induction was measured using Caspase-Glo® 3/7 assay (Promega). 100 µl of CellTiter-Glo luciferase substrate or Caspase 3/7 assay were mixed with 100 µl of culture medium in the plate containing the HLCs. After incubation 100 µl of the mixture was transferred into a white 96-well plate and luminescence was measured using a multiplex plate reader (GloMax Explorer, Promega).

CYP P450 activity

CYP 3A and CYP 1A2 activity were measured on HLCs at day 18 by using the P450-Glo™ assay (Promega). CYP 3A (1:20) and CYP 1A2 (1:50) substrates were diluted in hepatocyte maturation medium and added to the HLCs for 5 37 °C in 5% (v/v) CO_2, plain medium with substrate was incubated in parallel to subtract background. After incubation, 50 µL of supernatant was collected and mixed with 50 µL of luciferin detection reagent in a white 96-well plate at room temperature in the dark for 20 min. Luminescence was measured using a multiplex plate reader (GloMax Explorer, Promega) and normalized per mg of protein (RLU/ml/mg) quantified by BCA assay.

Differential expression analysis

Following sequencing, mapping and gene counting was performed by our collaborators at NNRCO. Next, differential expression and pathway enrichment analysis were performed using R programming. DEseq2 package was used for DEGs quantification and pathway viewer package for pathway enrichment (Love et al., 2014). Analysis was performed comparing paracetamol + DMF versus paracetamol, p adjusted value >0.05 was chosen as a threshold to detect DEGs. Then, only genes that displayed log2 Fold Change ±0.58 were selected for downstream analysis; ±0.58 log2 Fold Change equals a 1.5 fold change gene expression (Quackenbush, 2002). Gene expression analysis was focused on the DMF + paracetamol versus paracetamol in the different treatments to facilitate the analysis.

Finally, Gene Set Enrichment Analysis (GSEA) from the analyzed data after DEseq2 was performed. GSEA evaluates gene expression changes at the level of gene sets to identify the relevant biological process involved with the expression changes (Subramanian et al., 2005). In combination with GSEA, the molecular signatures database (MSigDB) hallmarks gene sets were used for the enrichment analysis (Liberzon et al., 2015). MSigDB hallmarks consist of 50 refined gene sets involved in key biological processes involved in metabolism, proliferation, cell signaling, immune response, DNA damage, development, cell singling pathways and cellular components. By using MSigDB, RNA-seq results can be refined from gene lists into biological changes. For Zebrafish, gene names were converted into human homologs and GSEA-MSigDB analysis was performed.

High content imaging and analysis

Image acquisition was performed using the automated Operetta fluorescent microscope. In brief, plates were placed in the Operetta and several random fields of view were imaged per well. Cell segmentation for image analysis was performed using the Columbus image analysis software. Cell segmentation is a process were the different organelles of the cells are identified for feature identification. Cell segmentation was performed by a first identification of the nuclei followed by cytoplasm identification. Next, a quality control step was performed to exclude cells not segmented correctly based on area, roundness and intensity. Finally, cell features such as intensity, morphology and texture were quantified for each channel and each organelle segmented.

Immunofluorescence

To study Nrf2 modulation following compound administration, media change was performed using the Viaflow automatic pipette dispenser. To minimize heat shock, the plate holder, and tips from the Viaflow were preincubated to 37°C. In addition, culture medium containing the different treatments were prepared in a 96-well deep-well plate and preincubated for at least 6 hr in the same incubator as the HLCs. Nrf2 nuclear translocation dynamics was analyzed by treating HLCs at day 18 with DMF 10 µM and 50 µM. Plates were fixed and stained 0.5 h, 2 h, 6 h and 24 h post administration. Cell cultures in 96-well plates were fixed

in 4% paraformaldehyde in H_2O for 15 minutes at room temperature. Subsequently, fixed cells were washed twice with PBS at room temperature. Cell were blocked with 0.1% PBS-Tween containing 10% BSA for one hour, followed by an incubation with primary antibodies diluted in PBS-0.1% Tween/1% BSA at 4°C overnight (Key Resources Table). Then the cells were washed three times with PBS-0.1% Tween/1% BSA. Secondary antibody was diluted in PBS/0.1% Tween/1% BSA and incubated for 1 hr at room temperature in the dark. Finally, the cells were washed three times with PBS and the nuclei was stained using NucBlue for 5 minutes.

Mass spectrometry

HLCs at day 18 were treated with Paracetamol 30 mM (dissolved in DMSO) or Vehicle for 24 h. After incubation, cell supernatants were collected and snap frozen on dry ice. Media supplemented with 30mM Paracetamol without cell incubation served an internal control. Targeted analysis of paracetamol and its metabolites in cell media samples was carried out by automated extraction on a PPT+ plate with acetonitrile and analysis by LC-MS/MS alongside calibration standards. Briefly, calibration standards (0.0025-1000 ng) were prepared and cell media samples were added to individual wells of a 96-well PPT+ plate (Biotage, Sweden), enriched with Paracetamol-d4 (APAP-d4; 10 ng) and 10 ng APAP-SUL-d3 as internal standards. 0.4 mL acetonitrile was added to each well by an Extrahera liquid handling robot (Biotage, Sweden), the solvent was passed through the extraction plate using positive pressure and the eluate reduced to dryness under nitrogen on an SPE-Dry 96 dual concentrator (Biotage, Sweden). The dried residue was resuspended in Water:Methanol (70:30; 100 uL) and the plate sealed with a zone-free 96-well plate sealing film (Sigma-Aldrich, Gillingham, UK).

Analysis was carried out by liquid chromatography tandem mass spectrometry (LC-MS/MS). Liquid chromatographic separation of all components was achieved using an Acquity Classic UPLC (Waters, UK) on a BEH C18 (150 x 2.1 mm; 1.7 µm; Waters, UK) column, protected by a Kinetex KrudKatcher® (Phenomenex, UK) at 45°C and detected on a QTrap 5500 mass spectrometer (AB Sciex, UK) in multiple reaction monitoring. The mobile phase consisted of 0.1 % formic acid in water (A) and 0.1 % formic acid in methanol (B) at a flow rate of 0.5 mL/min. Gradient elution was achieved with a total run time of 7.5 minutes from 5% to 95% B. The mass spectrometer was operated in polarity switching electrospray mode (550°C, 5.5 kV). The analytes APAP-Glu, APAP-Sul, APAP-Cys, APAP and APAP-GSH eluted from the column at 2.9, 3.2, 3.6, 4.2 and 5 mins, respectively. In positive mode, transitions monitored for were *m/z* 152 à 110.0, 92.9 at 23 and 31 V and *m/z* 156.0 à 114.0, 97.0 at 23 and 23 V for APAP and APAP-d4, APAP-CYS and APAP-GSH, *m/z* 271.1 à 140.0, 182.0 at 35 and 35 V and *m/z* 457.2 à 140 at 33 V. For the negatively ionized acetaminophen metabolites APAP-SUL, APAP-GLU, APAP-GSH and the internal standard APAP-SUL-d3 *m/z* 229.8 à 107.0, 150.1 at 36 and 15 V, *m/z* 326.0 à113.0, 150.0 at 28, *m/z* 455.0à 272.0, 182.0 at 36 and 10 V and 10 V and *m/z* 233.0 à 109.5, 181.4 at 30 and 5 V, respectively.

Linear regression analysis was applied to the ratio of the peak area of the analyte to the internal standard using Analyst quantitation software and the amount of Paracetamol and its metabolites in the samples was calculated from the peak area ratio using the linear regression analysis equation.

mRNA extraction and sequencing

RNA used for sequencing was isolated using the Dynabeads mRNA DIRECT Purification Kit (Thermo Fisher Scientific) according to manufacturer's instructions. RNA integrity was determined by RNA ScreenTape Assay (Agilent) and quantified using he Qubit RNA HS Assay Kit (Thermo Fisher Scientific) according to manufacturer's instructions. Following RNA quality control, library preparation was performed using the QUANT SEQ 3′ mRNA-seq Library Prep Kit FWD HT for Illumina (Lexogen) according to manufacturer's instructions. 15 ng of RNA was used to prepare the libraries. Following library preparation, library size and concertation were calculated using the Qubit dsDNA HS Assay Kit (Thermo Fisher scientific) and DNA ScreenTape (Aligent). Samples were pooled in a 10 mM library for long-term storage. Library sequencing was performed using the NextSeq 500/550 High Output Kit (Illumina) on the NextSeq 500 (Illumina) according to the manufacturer's instructions.

Orientation tool for zebrafish imaging 3D printing

3D printing of the orientation tool was performed using the available files from Wittbrodt et al. (Wittbrodt et al., 2014). Base plate and columns pins were printed by 'CNCvac 3D Printing' in generic Standard ABS using 100 µM layers to ensure high quality finish.

Reagent preparation for HLC incubation

Dimethyl fumarate (Sigma) stock solutions of 50 mM were prepared freshly for each experiment in DMSO (Sigma). H_2O_2 (Sigma) 30% (w/w) (molar concentration of 9.79 mol/L) was diluted in HepatoZYME medium to obtain a final concentration of 1 mM, Paracetamol 2 M (Sigma) was prepared freshly for each experiment in DMSO. SB-431542 was resuspended in DMSO at 10 mM aliquoted and stored at −80°C, a fresh aliquot was used for each experiment.

RNA extraction and qPCR

Either cells or liver tissue was extracted using RNeasy Kit (Qiagen) following manufacturer's instructions. Next, 400 ug of RNA was converted into cDNA using the QuantiTect Reverse Transcription Kit (Qiagen) accordingly to manufacturer's instructions. cDNA was diluted 1:10 prior qPCR analysis. qPCR was performed by using Taqman Fast Advance Mastermix and Taqman compatible primers in a Roche LightCycler480 according to the manufacturer's instructions.

DMF + paracetamol treatment time points

This paper describes multiple combinations of DMF +/− Paracetamol treatments in HLCs. This section aims to clarify when DMF was added at different experimental sets. For the Nrf2 nuclear translocation, DMF 10 μM or other compounds were added to multiple plates at the same and on each time point described on the manuscript, a plate was fixed. Staining was performed when all plates were fixed. For the DMF pre-treatment set of experiments, DMF 10 μM or NAC 1 mM were added to the cells for 24 hr, after incubation, media replacement was performed with fresh media containing Paracetamol 30 mM was added for further 24 hr. For the DMF post-treatment set of experiments, Paracetamol 30 mM was added to the cells for 24 hr, after incubation, media replacement was performed with fresh media containing DMF 10 μM, NAC 1 mM or SB-431542 10 μM were added for further 24 hr.

Zebrafish lines and husbandry

Experiments were conducted in accordance with the United Kingdom Animals (Scientific Procedures) Act 1986 in a United Kingdom Home Office-approved establishment. Zebrafish (Danio rerio) were maintained at 28.5°C, using standard procedures (Westerfield, 2007). Established lines used were WIK and Tg(-2.8 lfabp:GFP)), where GFP is green fluorescent protein (Her et al., 2003; Vliegenthart et al., 2017). All experiments were terminated at day 5 days post-fertilization (d.p.f.).

Zebrafish chemical exposure

The wild-type WIK line was used to optimize paracetamol-induced toxicity and dimethyl fumarate dosage. Unless otherwise stated, larvae were maintained at 28.5°C in 50 mL conditioned water (CW), treatments were carried out for 48 hr (3–5 d.p.f.). Single Tg(-2.8lfabp:GFP)) Zebrafish larvae per well were positioned into a black V-shape 96-well plate for 48 hr (3–5 days postfertilization (dpf)). At day 5, total fluorescence was measured using a fluorescence plate reader (ex/em 485/520).

Zebrafish high-throughput live imaging

Single larvae were oriented into a 96-well plate with 150 μL agar (0.75%, wt/vol) containing 84 mg/l MS-222. An orientation tool was 3D printed. Briefly, 0.75%, wt/vol agar was added into the 96-well plate following the positioning of the orientation tool (Figure S5). Once the agar was set, removal of the orientation tool creating an agar V shape where the larvae could be positioned. Imaging was performed using the operetta microscope, and image analysis was performed using Colomus software where supervised machine learning was used for automatic fish and liver recognition and analysis.

Zebrafish plate reader fluorescence quantification

Total fluorescence was detected using a fluorescence plate reader was used to detect changes in GFP signal. Paracetamol 10mM for 48 hr was used to quantify fluorescence decrease upon liver damage. Single larvae were introduced into a well of a black 96-well plate after treatment for fluorescence quantification. Wild-type larvae were used to subtract larvae autofluorescence.

Zebrafish RNA isolation and characterization

RNA was isolated from single embryos using the MIRneasy micro kit (Qiagen). RNA quality was measured by the RNA integrity number (RIN) using the TapeStation system. RIN is an algorithm used to assess RNA integrity by gel electrophoresis. Only samples that displayed RIN score >7 were Library preparation was performed using Lexogen's QuantSeq kit FWD HT. This kit allows a high-throughput library preparation and sample multiplexing generating Illumina-compatible libraries. Library size generated from this kit should be between 200 and 350 base pairs (bp). After sample multiplexing, a final library was generated. Library size was measured by TapeStation DNA electrophoresis. Library size was within the recommended size with a mean of 262 bp. Sequencing was performed using Illumina NextSeq 500 System with NextSeq 500/550 high output kit of 75 cycles. Library preparation and sequencing was performed at Novo Nordisk Research Center Oxford (NNRCO).

QUANTIFICATION AND STATISTICAL ANALYSIS

Statistical analysis

One-way ANOVA test and post-hoc Tukey multiple-comparison test was used for experiments that contained more than two groups. For groups of two, Unpaired two-sided t test was performed. Statistical analysis was performed using GraphPad Prism software.